Since January 2020 Elsevier has created a COVID-19 resource centre with free information in English and Mandarin on the novel coronavirus COVID-19. The COVID-19 resource centre is hosted on Elsevier Connect, the company's public news and information website.

Biochemical Engineering Journal 187 (2022) 108596

Contents lists available at ScienceDirect

Biochemical Engineering Journal

journal homepage: www.elsevier.com/locate/bej

Regular article

Engineered multivalent self-assembled binder protein against SARS-CoV-2 RBD

Dustin Britton [a,1], Kamia Punia [a,1], Farbod Mahmoudinobar [a,b], Takuya Tada [c], Xunqing Jiang [d], P. Douglas Renfrew [b], Richard Bonneau [b,e,f,g], Nathaniel R. Landau [c], Xiang-Peng Kong [d], Jin Kim Montclare [a,h,i,j,*]

[a] Department of Chemical and Biomolecular Engineering, New York University Tandon School of Engineering, Brooklyn, New York 11201, USA
[b] Center for Computational Biology, Flatiron Institute, New York, New York 10010, USA
[c] Department of Microbiology, NYU, Grossman School of Medicine, New York, New York 10016, USA
[d] Department of Biochemistry and Molecular Pharmacology, New York University Grossman School of Medicine, New York, New York 10016, USA
[e] Center for Genomics and Systems Biology, New York University, New York, New York 10003, USA
[f] Courant Institute of Mathematical Sciences, Computer Science Department, New York University, New York, New York 10009, USA
[g] Center for Data Science, New York University, New York, New York 10011, USA
[h] Bernard and Irene Schwartz Center for Biomedical Imaging, Department of Radiology, New York University School of Medicine, New York, New York 10016, USA
[i] Department of Chemistry, New York University, New York, New York 10012, USA
[j] Department of Biomaterials, New York University College of Dentistry, New York, New York 10010, USA

ARTICLE INFO

Keywords:
Protein engineering
SARS-CoV-2
Diagnostic
Therapeutic
Antibody-mimic

ABSTRACT

Severe acute respiratory syndrome coronavirus 2 (SARS-CoV-2) has caused a global pandemic since December 2019, and with it, a push for innovations in rapid testing and neutralizing antibody treatments in an effort to solve the spread and fatality of the disease. One such solution to both of these prevailing issues is targeting the interaction of SARS-CoV-2 spike receptor binding domain (RBD) with the human angiotensin-converting enzyme 2 (ACE2) receptor protein. Structural studies have shown that the N-terminal alpha-helix comprised of the first 23 residues of ACE2 plays an important role in this interaction. Where it is typical to design a binding domain to fit a target, we have engineered a protein that relies on multivalency rather than the sensitivity of a monomeric ligand to provide avidity to its target by fusing the N-terminal helix of ACE2 to the coiled-coil domain of the cartilage oligomeric matrix protein. The resulting ACE-MAP is able to bind to the SARS-CoV-2 RBD with improved binding affinity, is expressible in *E. coli*, and is thermally stable and relatively small (62 kDa). These properties suggest ACE-MAP and the MAP scaffold to be a promising route towards developing future diagnostics and therapeutics to SARS-CoV-2.

1. Introduction

The COVID-19 pandemic caused by severe acute respiratory syndrome coronavirus 2 (SARS-CoV-2) has, since December 2019, caused over 6 million deaths with over 500 million confirmed cases worldwide [1]. Great strides have been made through innovations in rapid testing and neutralizing antibody treatments in an effort to control the spread and fatality of the disease [2–4]. However, the lack of immediate widespread testing at the beginning of the pandemic has proven fatal [5]. The need for widely available therapies is also clear. If an infected person reaches the stage at which hospitalization is necessary, the COVID-19 patient faces a 21% death rate, more than five times greater than that of influenza [6]. Hospitalization has also been linked to higher viral titers in patients [7]. In terms of surveillance of the virus, testing of SARS-CoV-2 has relied on specialized instruments in addition to costly reagents and supplies for carrying out the reactions [8]. Lateral flow assays (LFAs) and enzyme-linked immunosorbent assays (ELISA), represent a point-of-care test for a simple, inexpensive, and fast diagnosis that predominantly relies on protein-protein interactions (PPIs) [2, 9].

* Corresponding author at: Department of Chemical and Biomolecular Engineering, New York University Tandon School of Engineering, Brooklyn, New York 11201, USA.
E-mail address: montclare@nyu.edu (J.K. Montclare).
[1] Authors contributed equally to this work.

https://doi.org/10.1016/j.bej.2022.108596
Received 13 June 2022; Received in revised form 2 August 2022; Accepted 17 August 2022
Available online 23 August 2022
1369-703X/

During infection by SARS-CoV-2, the spike (S) protein on the virus surface recognizes the peptidase domain (PD) of the angiotensin-converting enzyme 2 (ACE2) of the host [10]. Structural studies reveal that the N-terminal alpha-helix (residues 1–23) of human ACE2 receptor is critical to binding the S1 receptor binding domain (RBD) of SARS-CoV-2 [11–13]. Recently engineered recombinant ACE2 exhibits an increased avidity to SARS-CoV-2 compared to the wild-type [11,14,15]. Recombinant ACE2 has also been proven to block early infection [16]. However, recent studies have also shown that isolation of this alpha-helix as an antibody or protein domain mimic (PDM) provides weak protein-protein interaction with the SARS-CoV-2 RBD [13,17]. With this in mind, we have been inspired by nature's approach to design an antibody against a specific target to create a unique platform for engineering a stable, high-affinity PDM.

In the lifetime of an antibody's development, a disulfide bonded heavy and light chains self-assemble into a multivalent structure [18]. The multivalency of the protein provides a jump start in the race to increased affinity before undergoing its own evolutionary process, affinity maturation, to become a highly sensitive protein binder to a specific target [19]. Multivalency has proven to be an effective strategy to increase sensitivity and specificity of PPIs including multivalent displays of the SARS-CoV-2 RBDs and nanobodies against SARS-CoV-2 [20–25]. Whereas previously designed PDMs against the SARS-CoV-2 have used a variety of design techniques to mature affinity [11,15,17,26], we engineer high affinity via a multivalent protein design derived from a self-assembling protein domain (Fig. 1a). Recently, multivalent protein fusions have been developed bearing the coiled-coil domain of the cartilage oligomeric matrix protein (C) – a protein our lab has studied extensively [27,28] to create functional nanomaterials [29–34]. Here we describe the results of an ACE2 mimicking multivalent assembled protein (ACE-MAP) where the N-terminal alpha-helix (ACE_{BINDER}) is joined with a computationally designed kinked linker to C (Fig. 1b, Table A1) leading to high binding affinity of SARS-CoV-2 RBD for future applications as a biosensor or therapeutic.

2. Results and discussion

2.1. Computational design

Initial structure of C protein was taken from PDBID 3V2P and the 23-residue "binder protein" was taken from residues 21–44 of chain B in PDB 6M17, which was shown to have micromolar affinity to SARS-CoV-2 RBD [13]. In order to fuse the C and ACE_{BINDER} (derived from the N-terminal α-helix of ACE2), a series of alpha-helix forming rigid linkers consisting of $[EAAAK]_n$, (n = 2,3,4) motifs [35] were designed computationally using Rosetta [36] (data not shown). Initial monomeric structure of ACE-MAP was made in PyMOL [37] (Schrodinger). Using the symmetry information taken from PDBID 3V2P and Rosetta's symmetric modeling protocol [38], a pentameric structure was produced and relaxed with the FastRelax protocol and REF2015 score function [39]. The first five residues in the linker region were manually designed to provide a kink at the junction of C domain and linker, which provided an opening for binding to multiple S-RBDs (Fig. 1b). To further improve the chance of ACE-MAP•S-RBD interaction, different lengths of the linker sequence were modeled to ensure that the residues involved in ACE2 binding (Q24, T27, K31, E35, D38, Y41) [40] were on the outer surface of ACE-MAP. A linker sequence with 20 residues was chosen that provides adequate length and bend for an exposed binding domain where increasing n = 2 repeats of [EAAAK] exhibited the best Rosetta score per protein length (Table A2).

2.2. Binding affinity to SARS-CoV-2 RBD by enzyme-linked immunoassay (ELISA)

The binding affinity of ACE-MAP was tested against SARS-CoV-2 RBD (Fig. 2). ELISA protocol established by the Krammer Lab [41] and total binding saturation kinetics were used to determine the maximum saturation (B_{max}) and binding affinities (K_d) values. ACE-MAP exhibited a K_d of 620 pM. As a negative control, no detectable binding was observed for the parent protein, C (Fig. A1). ELISA assay was performed for ACE_{BINDER} using ACE_{BINDER} to seed the plate and SARS-COV-2 RBD as a primary antibody to avoid the impact of a tag on the ACE_{BINDER} affinity. Most notably, when applied without the MAP scaffold, ACE_{BINDER} did not show any detectable binding activity (Fig. A2), confirming previously reported inactivity of similarly derived binder sequences from ACE2 [13,26]. When compared to full length ACE2, which possessed a K_d of 11.7 nM, ACE-MAP was 19-fold better at binding SARS-CoV-2 RBD. This demonstrates that the presence of the fusion ACE_{BINDER} to the multivalent scaffold is crucial for affinity to the target. Compared to previously designed binders to SARS-CoV-2 RBD

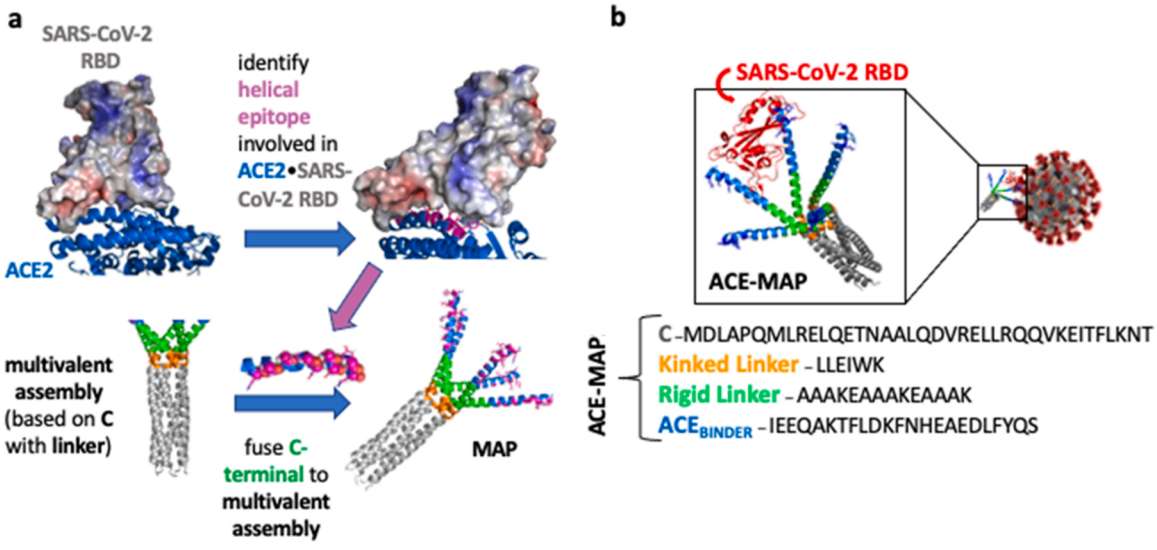

Fig. 1. a) Schematic for the MAP design strategy used to generate a scaffold for the ACE2 protein linker using SARS-CoV-2 RBD as a target. b) Cartoon representation of computationally designed ACE-MAP. C, kink, linker and binder protein are shown in grey, orange, green and blue color respectively. The residues involved in binding to SARS-CoV-2 RBD, shown in red, are shown in stick representation and dark blue color. (For interpretation of the references to colour in this figure legend, the reader is referred to the web version of this article.)

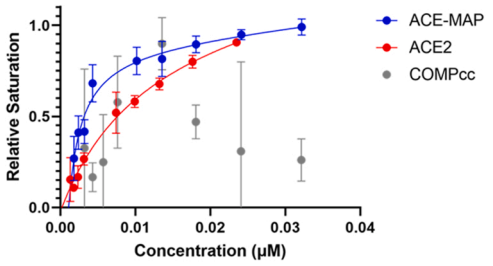

Fig. 2. Binding of ACE-MAP (blue) vs full length ACE2 (red) vs COMPcc (grey) as a function of SARS-CoV-2 RBD concentration measured by ELISA. Error bars represent the standard error of three independent trials. (For interpretation of the references to colour in this figure legend, the reader is referred to the web version of this article.)

ranging from 970 nM [26] to 100 pM [15], ACE-MAP was within the range and uniquely without further modification.

2.3. Structure and thermostability

Structural studies of ACE-MAP and ACE_{BINDER} were performed via circular dichroism spectroscopy. Wavelength scans performed at 25 °C revealed a double-minima of − 17,000 ± 700 deg•cm^2•dmol^{-1} 208 nm and − 16,000 ± 600 deg•cm^2•dmol^{-1} at 222 nm, indicative of helical conformation (Fig. 3a).

Analysis via CONTIN illustrated secondary structure of 50.2 ± 2.0 % helical content (Table A3). Relative to the parent C, which was reported to possess 70% helicity [42], a loss in structure was observed due to the addition of the linker and ACE_{BINDER}. Notably, the presence of the multivalent scaffold doubled the helical content when compared to ACE_{BINDER} which revealed only 35% helicity (Fig. A3, Table A4). To determine the stability of ACE-MAP, a temperature scan was carried out from 25 °C to 85 °C (Fig. 3a). While the parent C demonstrated a melting temperature of at 60 °C [43], ACE-MAP revealed a slight increase in stability with a T_m of 64.18 ± 0.87 °C relative to C. In contrast, ACE_{BINDER} revealed a lower T_m of 55.2 °C (Fig. A3).

To assess the extent of n-oligomerization due to the coiled-coil domain, BS^3 crosslinking of ACE-MAP was employed. After running the sample on a 12% SDS-PAGE, the gel was subjected to western blot analysis and imaged (Fig. 3b). Corresponding analysis software was used to quantify the band position and purity revealing a single protein band at approximately 62 kDa indicating n-oligomerization of n = 5 (pentamer) only as compared to ACE-MAP without BS^3 crosslinking (Figs. A4-A6).

The fusion of ACE_{BINDER} by a kinked linker has resulted in a similarly thermostable protein relative to its C counterpart [42]. In comparison, C with all cysteine residues (C48 and C54) mutated to serines (denoted as C^{SS}) reduces the melting temperature of C^{SS} to 45 °C [27]. Thus, despite the reduced helical secondary structure, likely due to the kinked region of ACE-MAP reducing the fraction of coiled-coil structure contribution, ACE-MAP maintains a T_m higher than C^{SS} and a T_m more characteristic to wild-type C [42,44]. Interchain disulfide-bond formation is a property only characteristic of a parallel n = 5 oligomer revealing that similarly ACE-MAP is likely to exist in the pentameric coiled-coil conformation [45–47]. Also of importance, is that the strong alpha-helical structure of C may lend itself as a scaffold that stabilizes the ACE_{BINDER} region to become functional against the SARS-CoV-2 RBD. The secondary structural data shown here elucidates this picture where ACE_{BINDER} possess just half the helical content of ACE-MAP. Previously, optimization of the domain's helicity only creates a modest improvement in binding affinity [17]. In addition to the pentamerization after BS^3 crosslinking, we deduce that the multivalency created by ACE-MAP through oligomerization of the C domain is critical for the increased binding affinity in comparison to ACE_{BINDER} [13,17] and ACE2 (**Section 2.2**). The increase in affinity and stability at high temperatures bodes well for future studies into applications of ACE-MAP as a stable biosensor or therapeutic.

2.4. Neutralization

ACE-MAP was tested for neutralization of SARS-CoV-2 B.1.1.7 (Delta variant) using a lentiviral pseudotyped assay (Fig. 4, Tables A4–A7). Inhibitor vs. normalized response kinetics were used to determine the IC50 values. While higher concentrations of ACE-MAP and ACE_{BINDER} exhibited increased infectivity, the high concentration of protein produced noise in the data. Thus, due to protein concentration limits and effects of protein oversaturation in the assay, ACE-MAP IC50 was projected from concentrations inhibiting > 50% infectivity of SARS-CoV-2 pseudotyped virus, which might produce some error in exact IC50 values. From the assay, while ACE-MAP demonstrated stronger inhibition of SARS-CoV-2 than ACE_{BINDER}, it was less potent than ACE2. Direct comparison of the IC50 values revealed that ACE-MAP possessed a 16.7-fold improvement in neutralization activity to ACE_{BINDER} with IC50 values of 1.05 μM and 18 μM, respectively (Fig. 4). In comparison, full-length ACE2 exhibited a much stronger ability to inhibit infectivity with

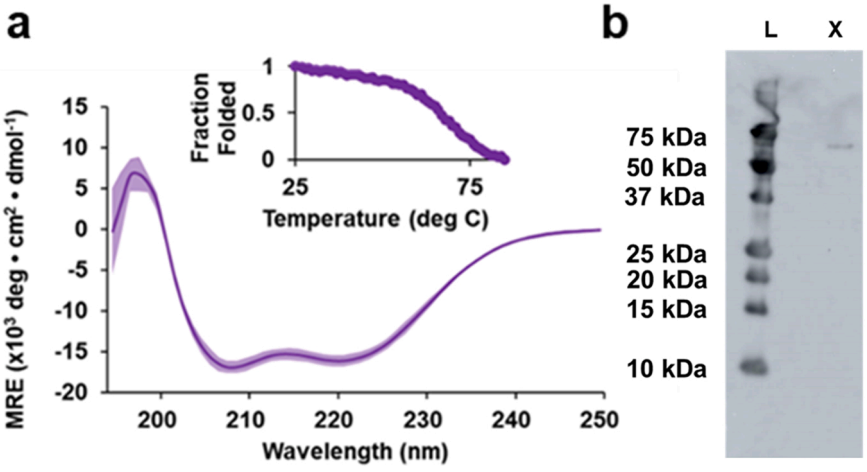

Fig. 3. a) Wavelength scan of ACE-MAP performed at 25 °C. Dark band – average MRE. Light shadow – ± standard deviation from average MRE inset: Representative ACE-MAP sample data of relative fraction folded using MRE at 222 nm wavelength from 25 °C to 85 °C b) Western blot from 12 % SDS-PAGE of ACE-MAP after BS^3. Image Analysis reveals intensity is approximately 62.2 kDa molecular weight corresponding to a pentamer self-assembly.

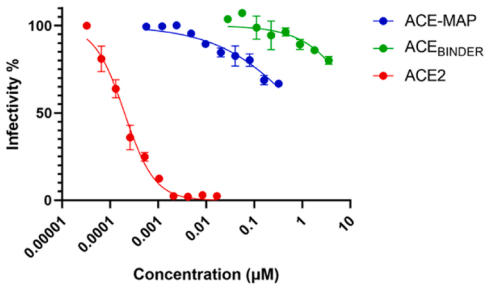

Fig. 4. SARS-COV-2 pseudotyped lentiviral neutralization fitted with Inhibitor vs. Normalized Response Kinetics using Prism 7 (Graphpad) of ACE-MAP (blue) and ACE$_{BINDER}$ (green) and ACE2 (red). (For interpretation of the references to colour in this figure legend, the reader is referred to the web version of this article.)

an IC50 value of 1.8 nM, a 573-fold improvement over ACE-MAP.

The large improvement of ACE-MAP to its parent protein, ACE$_{BINDER}$, supports ACE-MAP as a scaffold towards improved protein-protein targeting. The relative response points towards relationship between the structural function of the RBD as compared to a virion. While ACE-MAP shows strong affinity towards the RBD in vitro, the weaker neutralization activity when compared to ACE2 indicates that the larger virion may provide additional challenges such as competing intermolecular interactions, inhomogenous spatial organization, environment-dependent thermodynamic stability [48] and glycosylation [49]. As has often been introduced in the development of effective PDM IC50s, improvements upon the original protein engineered design will be needed to generate an effective agent in vivo [50]. Despite this, ACE-MAP shows a strong improvement over its parent ACE$_{BINDER}$ in neutralization of SARS-CoV-2.

Described in this work is a coiled-coil self-assembled fusion protein capable of binding to SARS-CoV-2 RBD at picomolar affinity. Its characterization has revealed insights into the utility of multivalent alpha-helical binders for this and future coronavirus variants. Several proteins and antibodies have been recently generated to bind to SARS-CoV-2 RBD [3,4,15,24,26,51,52]. These proteins tend to use either mammalian expression systems and/or be $>$ 140 kDa. The protein binders that have been computationally designed to increase the avidity to SARS-CoV-2 based on ACE2 possess K_d values ranging from 970 nM [26] to 100 pM [15].

E. coli expression systems have the unparalleled advantage of low cost, rapid growth, and good productivity; however, it is a host that is out of reach for many recombinant proteins $>$ 60 kDa, and especially antibodies, that require post-translational modifications [53–55]. In our studies, ACE-MAP yields 74 $\pm$ 9 μg/mL (n = 3) from 400 mL cultures measured by BCA assay following purification and concentration. *E.* coli expression systems tend to yield functional Fab fragments in the range of 400–800 μg (in 400 mL culture) [56] using shake flasks indicating that our yield should be improved for a comparable advantage. Thus, expression of our construct needs to further be optimized to provide improved yields whereas *E. coli* expression systems may often be enhanced with tailored expression time, bioreactor design, temperature, and gene vectors [56,57]. While ACE-MAP exhibits a strong affinity to SARS-CoV-2 RBD like antibodies, it possesses the advantage of soluble expression in *E. coli*, and a significantly smaller size – 12 kDa as a monomer (62 kDa as a pentamer).

Other small proteins or peptides being produced against SARS-CoV-2 RBD suffer from poor binding affinities to the SARS-CoV-2 RBD. Pentelute and coworkers have reported that a series of peptide binders designed against SARS-CoV-2 RBD range from 80 to 970 nM [26]. They have also previously reported that the same sequence used here, ACE-$_{BINDER}$, shows little to no binding affinity to SARS-CoV-2 [13] where we additionally demonstrate ACE$_{BINDER}$ to have low neutralization activity with an IC50 value of 18.0 μM (Fig. 4). Karoyan et al. have investigated and optimized the ACE$_{BINDER}$ sequence (to note they have included the first 27 residues) by retaining important residues and stabilizing its alpha helicity through iterative residue scanning [17]. As a result they have shown agreement that the native ACE$_{BINDER}$ sequence does not produce binding, while their optimized peptides produce up to approximately 3-fold improvement in binding affinity by Biolayer Interferometry compared to ACE2 [17]. Conversely, Baker and co-workers have reported several 'minibinders' that are capable of tight IC50 affinities; an increase in affinity is achieved by several rounds of mutagenesis using a ACE2 scaffolded design, followed by tethering another copy as dimer and trimer [15]. In a follow-up to these mini-binders, Baker and coworkers report multivalent heterotrimers to develop escape resistance while maintaining impressive IC50 affinities [25]. Our approach fundamentally differs from such prior work as the tethering or multivalency is part of the design from the outset. ACE-MAP joins only a handful of other recombinant PDMs that bind to SARS-COV-2 RBD [11,15,17,25,26]. Moreover, the conservation of the ACE2 binding sequence in ACE-MAP may prove resilient against mutant escape variants and future coronaviruses.

3. Conclusions

We have biosynthesized ACE-MAP, a small binder protein against SARS-CoV-2 RBD using a fusion of ACE$_{BINDER}$ to C via a computationally designed kinked linker. ACE-MAP has increased thermostability compared to C [27] and increased binding affinity through multivalency compared to the ACE$_{BINDER}$ region as previously reported [13]. ACE-MAP furthermore demonstrates the utility of generating a PDM utilizing multivalency as the source of high affinity. The increased efficacy of the protein and thermostability at room temperature indicates the utility of simple multivalent fusions. The high avidity of ACE-MAP to SARS-CoV-2 RBD by utilizing its target receptor, ACE2, reveals that ACE-MAP may be useful in a variety of biomedical applications such as the development of biosensors and therapeutics especially among the growing concern for SARS-CoV-2 mutant escape.

4. Methods and materials

4.1. Materials

Chemically competent AFIQ *E. coli* cells were gifted from David Tirrell at California Institute of Technology. ACE-MAP/pQE30 plasmid was cloned and purchased from Eurofins. Bacto-tryptone, sodium chloride, yeast extract, tryptic soy agar, ampicillin, chloramphenicol, sodium phosphate dibasic anhydrous (Na_2HPO_4), sodium hydroxide (NaOH), dextrose monohydrate (D-glucose), magnesium sulfate, calcium chloride ($CaCl_2$), manganese chloride tetrahydrate ($MnCl_20.4H_2O$), cobaltous chloride hexahydrate ($CoCl_20.6H_2O$), isopropyl β-D-1-thiogalactopyranoside (IPTG), Pierce bicinchoninic acid (BCA) assay kit, Pierce snakeskin dialysis tubing 3.5 K MWCO, sodium dodecyl sulfate, Pierce C18 tips with 10 μL bed, bissulfosuccinimidyl suberrate (BS^3), ascorbic acid, Immulon 4 HBX ninety-six well plates, Nunc ninety-six well plates, Dulbecco's Modified Eagle medium (DMEM), Nunc EasYFlask Cell Culture Flasks, Quant-iT PicoGreen dsDNA Assay Kit, IL-6 Mouse ELISA Kit, Pierce High Capacity Endotoxin Removal Spin Columns, and ELISA wash buffer (30X) were acquired from Thermo Fisher Scientific. The twenty naturally occurring amino acids, thiamine hydrochloride (vitamin B), dimethylsulfoxide (DMSO), and 3,3′,5,5′-tetramethylbenzidine (TMB) were purchased from Sigma Aldrich. Hydrochloric acid (HCl), Coomassie® Brilliant Blue G-250, and milk powder (non-fat, skimmed) were purchased from VWR. HiTrap Q HP 5 mL columns for protein purification were purchased from GE Healthcare Life Sciences. Macrosep and Microsep Advance Centrifugal Devices 3 K molecular weight cutoff (MWCO) and 0.2 μm syringe filters were purchased from PALL. Acrylamide/bis solution (30 %) 29:1, Mini Trans-Blot filer paper, Trans-Blot Transfer Medium (nitrocellulose

membrane), and natural polypeptide sodium dodecyl sulphate–polyacrylamide gel electrophoresis (SDS-PAGE) standard were purchased from Bio-Rad, and Dulbecco's phosphate buffered saline were purchased from ATCC.

4.2. Methods

4.2.1. ACE-MAP expression and purification

ACE-MAP protein was expressed in phenylalanine auxotrophic AFIQ *E. coli* cells. pQE30/ACE-MAP plasmid was transformed via heat shock in chemically competent AFIQ cells. Transformed cells were grown for 14–16 h at 37ºC on tryptic soy agar plates containing 200 μg/mL ampicillin and 35 μg/mL chloramphenicol. A single colony was inoculated in 16 mL supplemented M9 minimal medium (0.5 M Na_2HPO_4, 0.22 M KH_2PO_4, 0.08 M NaCl, and 0.18 M NH_4Cl) containing all 20 natural amino acids (100 μg/mL), ampicillin (200 μg/mL), chloramphenicol (35 μg/mL), vitamin B (35 μg/mL), D-glucose (100 μg/mL), magnesium sulfate (1 mM), calcium chloride (0.1 mM), and trace metals (0.02% v/v) and incubated at 37ºC and 350 rpm for 16 h. Following, 8 mL of the starter culture was added to 200 mL of supplemented M9 medium and incubated at 37ºC and 350 rpm until the optical density at 600 nm (OD_{600}) reached 0.7. Protein expression was induced with 200 μg/mL IPTG and incubated at 37ºC and 350 rpm for 3 h. After the expression, cells were harvested by centrifugation at 5000 × *g* at 4 ºC for 20 min in an Avanti J-25 centrifuge (Beckman Coulter) and stored at − 20ºC until purification. Expression of ACE-MAP was confirmed via 12% SDS-PAGE (Fig. A4).

Cell pellets were thawed and resuspended in Buffer A (50 mM Na_2HPO_4, 250 mM NaCl, 6 M urea, pH 8.0). Cells were lysed via Q500 probe sonicator (QSonica) at 65% amplitude, pulse on for 5 s and off for 30 s for a total of 2 min. The lysed cells were centrifuged at 11,000 × *g* for 45 min at 4 ºC to remove cell debris (Beckman Coulter). The supernatant was removed and purified using a syringe-pump driven IMAC Q Sepharose high performance 5 mL column (HiTrap Q HP 5, GE Health Sciences) charged with $CoCl_2$. Protein was eluted from the column using a gradient (0–100 %) of Buffer B (50 mM Na_2HPO_4, 250 mM NaCl, 6 M urea, 500 mM imidazole, pH 8.0) (Fig. A5). Elutions with pure protein were removed and dialyzed using a 3.5 kDa MWCO tubing at 4 ºC. Dialysis was performed using a step-wise decrease of urea from (three buckets from 3 M to 0.75 M urea) succeeded by six buckets with 0 M urea. The protein elutions were then concentrated to 1.5 mL using 3 kDa MWCO Macrosep and Microsep Advance centrifugal devices (Pall Corporation) at 2000 × *g*. Following, 500 μL volumes were injected into a Fast Purification Liquid Chromatography (FPLC, AKTA pure, GE Healthcare) using a Superdex 75 10/300 GL Size Exclusion Chromatography (SEC) column (GE Healthcare). Protein was eluted using phosphate buffered saline (PBS) pH 7.4. Pure fractions were determined using a 12% SDS-PAGE (Fig. A6) and protein concentration was determined using a bicinchoninic acid (BCA) assay with a standard curve based on bovine serum albumin concentrations.

4.2.2. SARS-CoV-2 RBD expression and purification

The plasmid used for protein expression and purification of SARS-CoV-2 RBD was constructed by insertion of a secretion signal, the coding sequence of a 5 A tag, RBD, and a 6xHis tag into an expression vector pVRC8400 (kindly provided by the Vaccine Research Center, National institute of Health). The gene construct was codon optimized for mammalian cell expression and synthesized by GenScript. The plasmid was transiently transfected into HEK293S cells for 5 days. Cell supernatants were filtered through 0.22-μm filters, loaded onto Ni-nitrilotriacetic acid (NTA) beads, and proteins were eluted with 600 mM imidazole. The elution was then dialyzed in PBS, flash frozen and stored at − 80 ºC.

4.2.3. Circular dichroism

Secondary structure of ACE-MAP and ACE_{BINDER} was measured using the Jasco J-815 CD spectrometer with a PTC-423S single position Peltier temperature control system. Wavelength scans of ACE-MAP (10 μM) were performed from 195 to 250 nm at 1 nm step sizes. ACE_{BINDER} was first reconstituted in DMSO prior to dilution in PBS. SEC was used to remove remaining DMSO prior to CD. Temperature scans were performed from 25 ºC to 85 ºC at 1 ºC step sizes. The mean residue ellipticity (MRE) and melting temperature (T_m) – using 222 nm for ACE-MAP and 214 nm for ACE_{BINDER} – were calculated as described in previous studies [27]. The secondary structure content (α-helicity, β-content, and unordered structure) was predicted with CONTIN/LL software [58–60].

4.2.4. Chemical crosslinking

Addition of 3 mM bis(sulfosuccinimidyl) suberate (BS^3) to a 10 μM concentration of ACE-MAP in PBS pH 7.4 was performed for chemical crosslinking to assess oligomerization. The reaction was allowed to incubate at room temperature and 300 rpm for 3 h in the dark on an Eppendorf Thermomixer C. The reaction was then quenched using 25 mM Tris HCl at pH 7.5 and sampled into a 12 % SDS-PAGE and oligomerization was confirmed using Western Blot analysis at a final concentration of 5 μM next to 5 μL of BioRad Precision Plus Protein Standard. To detect and analyze the oligomer bands, Amersham Imager 680 and corresponding analysis software (Cytiva Life Sciences) were used to detect and analyze relative intensities of oligomer bands.

4.2.5. Enzyme Linked Immunoassay

The ELISA protocol was adapted from previously established protocols [61]. A ninety-six well plate was coated overnight at 4 ℃ with 50 μL per well of a 2 μg/mL solution of SARS-CoV-2 RBD for ACE-MAP assay and with ACE_{BINDER} peptide for ACE_{BINDER} assay. ACE_{BINDER} was first reconstituted in DMSO prior to dilution in PBS. SEC was used to remove remaining DMSO prior to ELISA. The next morning, the coating solution was removed and 100 μL per well of 3 % non-fat milk prepared in PBS with 0.1 % Tween 20 (TPBS) was added to the plate at room temperature (RT) for 2 h as blocking solution. The blocking solution was removed and 100 μL of serial dilutions of ACE-MAP, C, and ACE2 proteins were added to plates coated with SARS-CoV-2 RBD for 2 h at RT. Serial dilutions of SARS-CoV-2 RBD were substituted as the primary antibody for plates coated with ACE_{BINDER}. The plates were washed three times at 200 μL volumes using 0.1 % TPBS. Approximately 100 μL of a 1:3000 anti-Histag horseradish peroxidase (HRP) conjugated secondary antibody (Sino Biological) was prepared in 0.1 % TPBS and added to each well for 1 h. Plates were then washed three times with 200 μL of 1x ELISA wash buffer (Thermo Scientific) and then air dried in a hood. While drying, TMB solution was prepared as described by Sigma Aldrich protocol. 1 mg/mL TMB was prepared in DMSO and then added to 0.05 mM citrate-phosphate buffer with 0.01 % hydrogen peroxide (0.01 %). Once completely dry, 100 μL of 3,3′,5,5′-tetramethylbenzidine (TMB) solution was added to the plates for 10 min. To quench the reaction, 50 μL of 3 M HCl was added to the plates. Absorbance at OD450 was immediately read using a microplate reader (BioTek Synergy H1).

4.2.6. Neutralization assay

ACE-MAP, ACE2, and ACE_{BINDER} were tested against SARS-CoV-2 using the previously established pseudotyped lentiviral neutralization assay [62] which is employed with ACE 0.293 T cells. Cells were plated in a 96 well tissue culture dish a 1×10^4 cells/well. ACE-MAP and ACE_{BINDER} was serially diluted and incubated with pseudotyped virus for 30 min before being added to the target cells. Cells were infected with pseudotyped SARS-Cov-2 and normalized for activity at MOI= 0.2. The next day, culture medium was removed and Nano-Glo luciferase substrate (Promega) was added before reading on an Envision 2103 microplate luminometer (PerkinElmer). Luciferase activity was normalized to the untreated cells and IC50 values were be calculated by fitting a sigmoidal nonlinear regression fit using inhibitor concentration vs. normalized response – Variable slope equation against concentration of protein using GraphPad Prism.

Funding sources

This work was supported by the National Science Foundation award numbers IIP-2031364, IIP- 1644681 and Army Research Office award number W911NF-19-1-0150.

Author contributions

The manuscript was written through contributions of all authors. All authors have given approval to the final version of the manuscript.

Declaration of Competing Interest

The authors declare that they have no known competing financial interests or personal relationships that could have appeared to influence the work reported in this paper.

Data Availability

Data will be made available on request.

Acknowledgments

We thank the National Academy of Engineering COVID-19 call for Engineering Action.

Appendix A. Supporting information

Supplementary data associated with this article can be found in the online version at doi:10.1016/j.bej.2022.108596.

References

[1] World Health Organization, 2020.
[2] F. Mahmoudinobar, D. Britton, J.K. Montclare, Protein-based lateral flow assays for COVID-19 detection, protein engineering, Des. Sel. 34 (2021).
[3] D.M. Weinreich, S. Sivapalasingam, T. Norton, S. Ali, H. Gao, R. Bhore, B.J. Musser, Y. Soo, D. Rofail, J. Im, C. Perry, C. Pan, R. Hosain, A. Mahmood, J.D. Davis, K. C. Turner, A.T. Hooper, J.D. Hamilton, A. Baum, C.A. Kyratsous, Y. Kim, A. Cook, W. Kampman, A. Kohli, Y. Sachdeva, X. Graber, B. Kowal, T. DiCioccio, N. Stahl, L. Lipsich, N. Braunstein, G. Herman, G.D. Yancopoulos, REGN-COV2, a neutralizing antibody cocktail, in outpatients with Covid-19, N. Engl. J. Med. 384 (2020) 238–251.
[4] J.D. Lundgren, B. Grund, C.E. Barkauskas, T.L. Holland, R.L. Gottlieb, U. Sandkovsky, S.M. Brown, K.U. Knowlton, W.H. Self, D.C. Files, M.K. Jain, T. Benfield, M.E. Bowdish, B.G. Leshnower, J.V. Baker, J.-U. Jensen, E.M. Gardner, A.A. Ginde, E.S. Harris, I.S. Johansen, N. Markowitz, M.A. Matthay, L. Østergaard, C.C. Chang, V.J. Davey, A. Goodman, E.S. Higgs, D.D. Murray, T.A. Murray, R. Paredes, M.K.B. Parmar, A.N. Phillips, C. Reilly, S. Sharma, R.L. Dewar, M. Teitelbaum, D. Wentworth, H. Cao, P. Klekotka, A.G. Babiker, A.C. Gelijns, V. L. Kan, M.N. Polizzotto, B.T. Thompson, H.C. Lane, J.D. Neaton, A neutralizing monoclonal antibody for hospitalized patients with Covid-19, N. Engl. J. Med. (2020). NEJMoa2033130.
[5] A.A. Dizioli, Michal, Bluedorn, John, COVID-19 Hits the Poor Harder, but Scaled-Up Testing Can Help, International Monetary Fund, 2020.
[6] Risk for In-Hospital Complications Associated with COVID-19 and Influenza - Veterans Health Administration, United States, October 1, 2018–May 31, 2020, centers for disease control and prevention, Cent. Dis. Control Prev. (2020).
[7] R. Wölfel, V.M. Corman, W. Guggemos, M. Seilmaier, S. Zange, M.A. Müller, D. Niemeyer, T.C. Jones, P. Vollmar, C. Rothe, M. Hoelscher, T. Bleicker, S. Brünink, J. Schneider, R. Ehmann, K. Zwirglmaier, C. Drosten, C. Wendtner, Virological assessment of hospitalized patients with COVID-2019, Nature 581 (2020) 465–469.
[8] C.B.F. Vogels, A.F. Brito, A.L. Wyllie, J.R. Fauver, I.M. Ott, C.C. Kalinich, M.E. Petrone, M.L. Landry, E.F. Foxman, N.D. Grubaugh, Analytical sensitivity and efficiency comparisons of SARS-COV-2 qRT-PCR assays medRxiv preprint (2020).
[9] J. Kim, M.A. Abdou, K. Zagorovsky, W.C.W. Chan, State of diagnosing infectious pathogens using colloidal nanomaterials, Biomaterials 146 (2017) 97–114.
[10] R. Yan, Y. Zhang, Y. Li, L. Xia, Y. Guo, Q. Zhou, Structural basis for the recognition of SARS-CoV-2 by full-length human ACE2, Science 367 (2020) 1444–1448.
[11] M. Romano, A. Ruggiero, F. Squeglia, R. Berisio, An engineered stable mini-protein to plug SARS-Cov-2 Spikes, bioRxiv, (2020) 2020.2004.2029.067728.
[12] D. Wrapp, N. Wang, K.S. Corbett, J.A. Goldsmith, C. Hsieh, O. Abiona, B. S. Graham, J.S. McLellan, Cryo-EM structure of the 2019-nCoV spike in the prefusion conformation, Science 367 (2020) 1260–1263.
[13] G. Zhang, S. Pomplun, A.R. Loftis, X. Tan, A. Loas, B.L. Pentelute, Investigation of ACE2 N-terminal fragments binding to SARS-CoV-2 Spike RBD, bioRxiv, (2020) 2020.2003.2019.999318.
[14] A. Glasgow, J. Glasgow, D. Limonta, P. Solomon, I. Lui, Y. Zhang, M.A. Nix, N. J. Rettko, S. Zha, R. Yamin, K. Kao, O.S. Rosenberg, J.V. Ravetch, A.P. Wiita, K. K. Leung, S.A. Lim, X.X. Zhou, T.C. Hobman, T. Kortemme, J.A. Wells, Engineered ACE2 receptor traps potently neutralize SARS-CoV-2, Proc. Natl. Acad. Sci. 117 (2020) 28046.
[15] L. Cao, I. Goreshnik, B. Coventry, J.B. Case, L. Miller, L. Kozodoy, R.E. Chen, L. Carter, A.C. Walls, Y.-J. Park, E.-M. Strauch, L. Stewart, M.S. Diamond, D. Veesler, D. Baker, De novo design of picomolar SARS-CoV-2 miniprotein inhibitors, Science 370 (2020) 426.
[16] V. Monteil, H. Kwon, P. Prado, A. Hagelkruys, R.A. Wimmer, M. Stahl, A. Leopoldi, E. Garreta, C. Hurtado Del Pozo, F. Prosper, J.P. Romero, G. Wirnsberger, H. Zhang, A.S. Slutsky, R. Conder, N. Montserrat, A. Mirazimi, J.M. Penninger, Inhibition of SARS-CoV-2 infections in engineered human tissues using clinical-grade soluble human ACE2, Cell 181 (2020) 905–913, e907.
[17] P. Karoyan, V. Vieillard, L. Gómez-Morales, E. Odile, A. Guihot, C.-E. Luyt, A. Denis, P. Grondin, O. Lequin, Human ACE2 peptide-mimics block SARS-CoV-2 pulmonary cells infection, Commun. Biol. 4 (2021) 197.
[18] M.L. Chiu, D.R. Goulet, A. Teplyakov, G.L. Gilliland, Antibody structure and function: the basis for engineering therapeutics, Antibodies 8 (2019) 55.
[19] F. Karush, Multivalent Binding and Functional Affinity, in: H.N. Eisen, R. A. Reisfeld (Eds.), Contemporary Topics in Molecular Immunology, Springer US, Boston, MA, 1976, pp. 217–228.
[20] T.K. Tan, P. Rijal, R. Rahikainen, A.H. Keeble, L. Schimanski, S. Hussain, R. Harvey, J.W.P. Hayes, J.C. Edwards, R.K. McLean, V. Martini, M. Pedrera, N. Thakur, C. Conceicao, I. Dietrich, H. Shelton, A. Ludi, G. Wilsden, C. Browning, A.K. Zagrajek, D. Bialy, S. Bhat, P. Stevenson-Leggett, P. Hollinghurst, M. Tully, K. Moffat, C. Chiu, R. Waters, A. Gray, M. Azhar, V. Mioulet, J. Newman, A. S. Asfor, A. Burman, S. Crossley, J.A. Hammond, E. Tchilian, B. Charleston, D. Bailey, T.J. Tuthill, S.P. Graham, H.M.E. Duyvesteyn, T. Malinauskas, J. Huo, J. A. Tree, K.R. Buttigieg, R.J. Owens, M.W. Carroll, R.S. Daniels, J.W. McCauley, D. I. Stuart, K.-Y.A. Huang, M. Howarth, A.R. Townsend, A COVID-19 vaccine candidate using SpyCatcher multimerization of the SARS-CoV-2 spike protein receptor-binding domain induces potent neutralising antibody responses, Nat. Commun. 12 (2021) 542.
[21] E. Zumbro, A. Alexander-Katz, Influence of binding site affinity patterns on binding of multivalent polymers, ACS Omega 5 (2020) 10774–10781.
[22] C. Chittasupho, Multivalent ligand: design principle for targeted therapeutic delivery approach, Ther. Deliv. 3 (2012) 1171–1187.
[23] M. Mammen, S.-K. Choi, G.M. Whitesides, Polyvalent interactions in biological systems: implications for design and use of multivalent ligands and inhibitors, Angew. Chem. Int. Ed. 37 (1998) 2754–2794.
[24] P.-A. Koenig, H. Das, H. Liu, B.M. Kümmerer, F.N. Gohr, L.-M. Jenster, L.D. J. Schiffelers, Y.M. Tesfamariam, M. Uchima, J.D. Wuerth, K. Gatterdam, N. Ruetalo, M.H. Christensen, C.I. Fandrey, S. Normann, J.M.P. Tödtmann, S. Pritzl, L. Hanke, J. Boos, M. Yuan, X. Zhu, J.L. Schmid-Burgk, H. Kato, M. Schindler, I.A. Wilson, M. Geyer, K.U. Ludwig, B.M. Hällberg, N.C. Wu, F. I. Schmidt, Structure-guided multivalent nanobodies block SARS-CoV-2 infection and suppress mutational escape, Science 371 (2021) eabe6230.
[25] C. Hunt Andrew, B. Case James, Y.-J. Park, L. Cao, K. Wu, C. Walls Alexandra, Z. Liu, E. Bowen John, H.-W. Yeh, S. Saini, L. Helms, T. Zhao Yan, T.-Y. Hsiang, N. Starr Tyler, I. Goreshnik, L. Kozodoy, L. Carter, R. Ravichandran, B. Green Lydia, L. Matochko Wadim, A. Thomson Christy, B. Vögeli, A. Krüger, A. VanBlargan Laura, E. Chen Rita, B. Ying, L. Bailey Adam, M. Kafai Natasha, E. Boyken Scott, A. Ljubetič, N. Edman, G. Ueda, M. Chow Cameron, M. Johnson, A. Addetia, M.-J. Navarro, N. Panpradist, M. Gale, S. Freedman Benjamin, D. Bloom Jesse, H. Ruohola-Baker, P.J. Whelan Sean, L. Stewart, S. Diamond Michael, D. Veesler, C. Jewett Michael, D. Baker, Multivalent designed proteins neutralize SARS-CoV-2 variants of concern and confer protection against infection in mice, Science Translational Medicine, 14 eabn1252.
[26] S. Pomplun, M. Jbara, A.J. Quartararo, G. Zhang, J.S. Brown, Y.-C. Lee, X. Ye, S. Hanna, B.L. Pentelute, De Novo discovery of high-affinity peptide binders for the SARS-CoV-2 spike protein, ACS Cent. Sci. 7 (2021) 156–163.
[27] S.K. Gunasekar, M. Asnani, C. Limbad, J.S. Haghpanah, W. Hom, H. Barra, S. Nanda, M. Lu, J.K. Montclare, N-terminal aliphatic residues dictate the structure, stability, assembly, and small molecule binding of the coiled-coil region of cartilage oligomeric matrix protein, Biochemistry 48 (2009) 8559–8567.
[28] L. Yin, A.S. Agustinus, C. Yuvienco, T. Miniashima, N.S. Schnabel, T. Kirsch, J. K. Montclare, Engineered coiled-coil protein for delivery of inverse agonist for osteoarthritis, Biomacromolecules 19 (2018) 1614–1624.
[29] L.K. Hill, J.A. Frezzo, P. Katyal, D.M. Hoang, Z.B. Youss, C. Xu, X. Xie, E. Delgado-Fukushima, Y.Z. Wadghiri, J.K. Montclare, Protein engineered nanoscale micelles for dynamic 19F magnetic resonance for therapeutic drug delivery, ACS Nano 13 (2019) 2969–2985.
[30] A.J. Olsen, J.S. Haghpanah, P. Katyal, N.S. Schnabel, M. Dai, N. Singh, R.S. Tu, J. K. Montclare, Protein Engineered Triblock Polymers Comprised of Two SADs: Enhanced Mechanical Properties and Binding Abilities, Biomacromolecues 19 (2018) 1552–1561.
[31] M. Dai, J.A. Frezzo, E. Sharma, R. Chen, N. Singh, C. Yuvienco, E. Caglar, S. Xiao, A. Saxena, J.K. Montclare, Engineered protein polymer-gold nanoparticle hybrid materials for small molecule delivery, J. Nanomed. Nanotechnol. (2016), https://doi.org/10.4172/2157-7439.1000356.

[32] M. Dai, J. Haghpanah, N. Singh, E.W. Roth, A. Liang, R.S. Tu, J.K. Montclare, Artificial protein block polymer libraries bearing two SADs: effects of elastin domain repeats, Biomacromolecules 12 (2011) 4240–4246.
[33] J.S. Haghpanah, C. Yuvienco, E.W. Roth, A. Liang, R.S. Tu, J.K. Montclare, Supramolecular assembly and small molecule recognition by genetically engineered protein block polymers composed of two SADs, Mol. Biosyst. 6 (2010) 1662–1667.
[34] J.S. Haghpanah, C. Yuvienco, D.E. Civay, H. Barra, P.J. Baker, S. Khapli, N. Voloshchuk, S.K. Gunasekar, M. Muthukumar, J.K. Montclare, Artificial protein block copolymers blocks comprising two distinct self-assembling domains, ChemBioChem 10 (2009) 2733–2735.
[35] X. Chen, J.L. Zaro, W.C. Shen, Fusion protein linkers: property, design and functionality, Adv. Drug Deliv. Rev. 65 (2013) 1357–1369.
[36] A. Leaver-Fay, M. Tyka, S.M. Lewis, O.F. Lange, J. Thompson, R. Jacak, K. Kaufman, P.D. Renfrew, C.A. Smith, W. Sheffler, I.W. Davis, S. Cooper, A. Treuille, D.J. Mandell, F. Richter, Y.E. Ban, S.J. Fleishman, J.E. Corn, D.E. Kim, S. Lyskov, M. Berrondo, S. Mentzer, Z. Popovic, J.J. Havranek, J. Karanicolas, R. Das, J. Meiler, T. Kortemme, J.J. Gray, B. Kuhlman, D. Baker, P. Bradley, ROSETTA3: an object-oriented software suite for the simulation and design of macromolecules, Methods Enzym. 487 (2011) 545–574.
[37] Pymol, The PyMOL Molecular Graphics System, Version 2.0 Shrödinger, LLC.
[38] F. DiMaio, A. Leaver-Fay, P. Bradley, D. Baker, I. André, Modeling symmetric macromolecular structures in Rosetta3, PloS One 6 (2011) e20450-e20450.
[39] R.F. Alford, A. Leaver-Fay, J.R. Jeliazkov, M.J. O'Meara, F.P. DiMaio, H. Park, M. V. Shapovalov, P.D. Renfrew, V.K. Mulligan, K. Kappel, J.W. Labonte, M.S. Pacella, R. Bonneau, P. Bradley, R.L. Dunbrack Jr., R. Das, D. Baker, B. Kuhlman, T. Kortemme, J.J. Gray, The rosetta all-atom energy function for macromolecular modeling and design, J. Chem. Theory Comput. 13 (2017) 3031–3048.
[40] J. Lan, J. Ge, J. Yu, S. Shan, H. Zhou, S. Fan, Q. Zhang, X. Shi, Q. Wang, L. Zhang, X. Wang, Crystal structure of the 2019-nCoV spike receptor-binding domain bound with the ACE2 receptor, bioRxiv, (2020) 2020.2002.2019.956235.
[41] F. Amanat, D. Stadlbauer, S. Strohmeier, T.H.O. Nguyen, V. Chromikova, M. McMahon, K. Jiang, G.A. Arunkumar, D. Jurczyszak, J. Polanco, M. Bermudez-Gonzalez, G. Kleiner, T. Aydillo, L. Miorin, D.S. Fierer, L.A. Lugo, E.M. Kojic, J. Stoever, S.T.H. Liu, C. Cunningham-Rundles, P.L. Felgner, T. Moran, A. García-Sastre, D. Caplivski, A.C. Cheng, K. Kedzierska, O. Vapalahti, J.M. Hepojoki, V. Simon, F. Krammer, A serological assay to detect SARS-CoV-2 seroconversion in humans, Nat. Med. 26 (2020) 1033–1036.
[42] A.V. Terskikh, S.A. Potekhin, T.N. Melnik, A.V. Kajava, Mutation Gln54Leu of the conserved polar residue in the interfacial coiled coil position (d) results in significant stabilization of the original structure of the COMP pentamerization domain, Lett. Pept. Sci. 4 (1997) 297–304.
[43] Y. Guo, D. Bozic, V.N. Malashkevich, R.A. Kammerer, T. Schulthess, J. Engel, All-trans retinol, vitamin D and other hydrophobic compounds bind in the axial pore of the five-stranded coiled-coil domain of cartilage oligomeric matrix protein, EMBO J. 17 (1998) 5265–5272.
[44] V.P. Efimov, A. Lustig, J. Engel, The thrombospondin-like chains of cartilage oligomeric matrix protein are assembled by a five-stranded α-helical bundle between residues 20 and 83, FEBS Lett. 341 (1994) 54–58.
[45] M. Mörgelin, D. Heinegård, J. Engel, M. Paulsson, Electron microscopy of native cartilage oligomeric matrix protein purified from the Swarm rat chondrosarcoma reveals a five-armed structure, J. Biol. Chem. 267 (1992) 6137–6141.
[46] E. Hedbom, P. Antonsson, A. Hjerpe, D. Aeschlimann, M. Paulsson, E. Rosa-Pimentel, Y. Sommarin, M. Wendel, A. Oldberg, D. Heinegård, Cartilage matrix proteins. An acidic oligomeric protein (COMP) detected only in cartilage, J. Biol. Chem. 267 (1992) 6132–6136.
[47] A.V. Kajava, Modeling of a five-stranded coiled coil structure for the assembly domain of the cartilage oligomeric matrix protein, Protein.: Struct., Funct., Bioinforma. 24 (1996) 218–226.
[48] K.S. Hingorani, L.M. Gierasch, Comparing protein folding in vitro and in vivo: foldability meets the fitness challenge, Curr. Opin. Struct. Biol. 24 (2014) 81–90.
[49] M.K. Leabman, Y.G. Meng, R.F. Kelley, L.E. DeForge, K.J. Cowan, S. Iyer, Effects of altered FcγR binding on antibody pharmacokinetics in cynomolgus monkeys, mAbs 5 (2013) 896–903.
[50] H. Lu, Q. Zhou, J. He, Z. Jiang, C. Peng, R. Tong, J. Shi, Recent advances in the development of protein–protein interactions modulators: mechanisms and clinical trials, Signal Transduct. Target. Ther. 5 (2020) 213.
[51] Y. Guo, L. Huang, G. Zhang, Y. Yao, H. Zhou, S. Shen, B. Shen, B. Li, X. Li, Q. Zhang, M. Chen, D. Chen, J. Wu, D. Fu, X. Zeng, M. Feng, C. Pi, Y. Wang, X. Zhou, M. Lu, Y. Li, Y. Fang, Y.-Y. Lu, X. Hu, S. Wang, W. Zhang, G. Gao, F. Adrian, Q. Wang, F. Yu, Y. Peng, A.G. Gabibov, J. Min, Y. Wang, H. Huang, A. Stepanov, W. Zhang, Y. Cai, J. Liu, Z. Yuan, C. Zhang, Z. Lou, F. Deng, H. Zhang, C. Shan, L. Schweizer, K. Sun, Z. Rao, A. SARS-CoV-2, neutralizing antibody with extensive Spike binding coverage and modified for optimal therapeutic outcomes, Nat. Commun. 12 (2021) 2623.
[52] F. Bertoglio, D. Meier, N. Langreder, S. Steinke, U. Rand, L. Simonelli, P.A. Heine, R. Ballmann, K.-T. Schneider, K.D.R. Roth, M. Ruschig, P. Riese, K. Eschke, Y. Kim, D. Schäckermann, M. Pedotti, P. Kuhn, S. Zock-Emmenthal, J. Wöhrle, N. Kilb, T. Herz, M. Becker, M. Grasshoff, E.V. Wenzel, G. Russo, A. Kröger, L. Brunotte, S. Ludwig, V. Fühner, S.D. Krämer, S. Dübel, L. Varani, G. Roth, L. Čičin-Šain, M. Schubert, M. Hust, SARS-CoV-2 neutralizing human recombinant antibodies selected from pre-pandemic healthy donors binding at RBD-ACE2 interface, Nat. Commun. 12 (2021) 1577.
[53] N.K. Tripathi, A. Shrivastava, Recent developments in bioprocessing of recombinant proteins: expression hosts and process development, Front. Bioeng. Biotechnol. 7 (2019).
[54] N.B. Mohammed, M.A.-H. Ahmed, S.B. Roop, M.M.A. Mohamed, *, A.I.R. Hassan, S.S. Kulvinder, A.B. Nabih, M.R. Elrashdy, Production of biopharmaceuticals in E. coli: current scenario and future perspectives, J. Microbiol. Biotechnol. 25 (2015) 953–962.
[55] S.K. Gupta, P. Shukla, Advanced technologies for improved expression of recombinant proteins in bacteria: perspectives and applications, Crit. Rev. Biotechnol. 36 (2016) 1089–1098.
[56] S. Huleani, M.R. Roberts, L. Beales, E.H. Papaioannou, Escherichia coli as an antibody expression host for the production of diagnostic proteins: significance and expression, Crit. Rev. Biotechnol. 42 (2022) 756–773.
[57] D.M. Francis, R. Page, Strategies to optimize protein expression in E. coli, Curr. Protoc. Protein Sci. (2010). Unit 5.24.21-29.
[58] N.J. Greenfield, Using circular dichroism spectra to estimate protein secondary structure, Nat. Protoc. 1 (2006) 2876–2890.
[59] S.W. Provencher, J. Glockner, Estimation of globular protein secondary structure from circular dichroism, Biochemistry 20 (1981) 33–37.
[60] N. Sreerama, S.Y. Venyaminov, R.W. Woody, Estimation of the number of alpha-helical and beta-strand segments in proteins using circular dichroism spectroscopy, Protein Sci. 8 (1999) 370–380.
[61] F. Amanat, K.M. White, L. Miorin, S. Strohmeier, M. McMahon, P. Meade, W.-C. Liu, R.A. Albrecht, V. Simon, L. Martinez-Sobrido, T. Moran, A. García-Sastre, F. Krammer, An in vitro microneutralization assay for SARS-CoV-2 serology and drug screening, Curr. Protoc. Microbiol 58 (2020) e108-e108.
[62] T. Tada, H. Zhou, B.M. Dcosta, M.I. Samanovic, M.J. Mulligan, N.R. Landau, Partial resistance of SARS-CoV-2 delta variants to vaccine-elicited antibodies and convalescent sera, iScience 24 (2021), 103341.